Modeling Method Based on Output-layer Structure Feedback Elman Neural Network and PID Decoupling Control of PVC Stripping Process

Hong-Yu Wang, Dong Wei *, Jie-Sheng Wang, Wei-Zhen Sun

Abstract—**The PVC stripping process is a complex industrial process with highly nonlinear and time varying. It is difficult to establish an accurate mathematical model due to multivariable, nonlinear, coupled and large hysteresis, etc. So the modeling method based on output-layer structure feedback Elman (OSF-Elman) neural network and PID decoupling control strategy of PVC stripping process is proposed. Firstly, the OSF-Elman neural network modeling method is proposed to establish the controlled object model with the actual operational data of the vinyl chloride stripping process. Then a neural network decentralized decoupling controller is used to decouple the stripping process to obtain two SISO systems (slurry flow - tower top temperature and steam flow-tower bottom temperature). Finally, the whale optimization algorithm (WOA) based PID controller is applied to the decoupled stripper system to achieve the effective performance for the PVC stripping process. The simulation results verify the effectiveness of the proposed integrated control strategy.**

Index Terms—**PVC stripping process; Elman neural network; PID decoupling control; Whale optimization algorithm**

I. Introduction

Polyvinyl chloride (PVC) is a large-scale basic chemical raw material. PVC is obtained by the polymerization reaction of vinyl chloride monomer. In order to ensure the quality of PVC resin, the polymerization conversion rate is generally controlled at 80%-90%. Unreacted vinyl chloride monomer is recovered by self-pressure, but the monomer about 1%-2% remains in the PVC slurry. Since the vinyl chloride monomer has certain toxicity, it must be further removed and recovered in the production. Removal of vinyl chloride remaining in the polyvinyl chloride resin can improve the quality of the polyvinyl chloride resin, reduce the production cost, and solve the problems of environmental pollution in the processing and use of plastics. In the current methods of removing excess VCM monomer from PVC slurry, the stripping process is very effective [1]. At present, most of the control researches on the PVC industry are in the stages of polymerization and rectification. The advanced control technologies, such as neural networks, fuzzy control, expert systems and predictive control, are widely used. The neural network based decoupling and nonlinear adaptive control are widely used in PVC production process [2-5]. A BP neural network decoupling controller was applied to the temperature control of a distillation column and the simulation results show that the algorithm is robust [2]. Aiming at the PVC fluidity bed drying process, a steady-state optimization model for the energy consumption was proposed based on the artificial neural network. Then the multi-variable state feedback control system was designed to effectively remove the correlation between the variables. The actual operation shows that the system has strong robustness and reaches the minimum energy consumption control index of the fluidity bed [3]. A advanced control method based on the neural network and the predictive control system was proposed aiming at the rectification tower so as to make the system have a small overshoot and a short response time [4]. A BP neural network decoupling controller was applied to the temperature control of the distillation column and the good robustness and control effect were realized [5].

Elman neural network is a dynamic neural network based on BP neural network. It stores the internal states and has the function of mapping dynamic characteristics so that the system has the adaption ability to the time-varying characteristics. Because most of the industrial production processes are dynamical, when a dynamic neural network such as BP neural network or RBF neural network is used, the ideal result is often not obtained. Therefore, in dealing with this kind of the complex industrial processes, in order to obtain the better reflection on the dynamic characteristics of the system, a dynamic neural network is required. The Elman neural network model was adopted to predict the Kappa value of pulp [6]. An Elman neural network was used to detect the fault of the motor fault, and the genetic algorithm (GA) was introduced to optimize the weights of the Elman neural network to further improve the detection performance [7].

Manuscript received December 27, 2019; revised March 5, 2020. This work was supported by the Basic Scientific Research Project of Institution of Higher Learning of Liaoning Province (Grant No. 2017FWDF10), and the Project by Liaoning Provincial Natural Science Foundation of China (Grant No. 20180550700 and 20190550263).

Hong-Yu Wang is a postgraduate student in the School of Electronic and Information Engineering, University of Science and Technology Liaoning, Anshan, 114051, PR China (e-mail: wanghongyuww @126.com).

Dong Wei is with the School of Electronic and Information Engineering, University of Science and Technology Liaoning, Anshan, 114051, PR China. (Corresponding author, phone: 86-0412-5929747; e-mail: asweidong@126.com).

Jie-Sheng Wang is with the School of Electronic and Information Engineering, University of Science and Technology Liaoning, Anshan, 114051, PR China. (e-mail: wang_jiesheng@126.com).

Wei-Zhen Sun is a postgraduate student in the School of Electronic and Information Engineering, University of Science and Technology Liaoning, Anshan, 114051, PR China. (e-mail: 851062813@qq.com).

The Elman neural network was used to predict the pressure of the emulsion pumping station and obtained good results [8]. The Elman neural network was adopted to predict the silicon content of steel mill blast furnace and the particle swarm optimization (PSO) algorithm was used to optimize the weights of Elman neural network so as to obtain a good prediction effect [9]. The Elman neural network was used for waste water treatment modeling, and the recursive least squares (RLS) and Kalman filters were used to update the linear and nonlinear parameters so as to improve the accuracy and generalization ability of the model [10].

Because the PVC stripping process is a production process with high non-linearity, strong coupling, and slow time-varying characteristics. The traditional modeling methods will result in an unsatisfactory model. However, there is a lack of research on advanced control methods for the stripping process in PVC production. The accurate mathematical model is difficult to establish, so it is difficult to achieve good control effects by traditional control methods. In this paper, based on the properties of the stripper process, considering the characteristics of the nonlinear fitting of the neural network and the ability to approximate arbitrary functions with arbitrary precision, an Elman neural network based modeling method and the decoupling method on the PVC stripping process are proposed. On the other hand, the whale optimization algorithm (WOA) is adopted to optimize the parameters of the decoupled PID controller. The simulation results show the effectiveness of the proposed strategy.

II. Technique of PVC Stripping Process

During the polymerization reaction process of vinyl chloride, according to different techniques and resin grades, the conversion rate of vinyl chloride is generally controlled at 80%-90%. Then the unreacted monomer is recovered in the kettle and dried by the sedimentation tank, but the resin remains in the finished product and a small amount of vinyl chloride monomer affects the quality of the product and increases the hazard when using plastic. In addition, the annual discharge of vinyl chloride into the atmosphere not only causes huge waste of raw materials, but also causes serious pollution to the environment. At present, the stripping process is very effective in removing excess VCM monomer from the PVC slurry. The technique flow of the PVC stripping process by using a sieve plate through a slab-type stripper is shown in Fig. 1. After the end of the polymerization reaction, the PVC slurry is first filtered, and then sent to the heat ex-changer by the slurry pump and is carried out the heat exchange with the purified PVC. The PVC slurry is sent to the top of the stripper and the PVC slurry is evenly sprayed onto the tray and flows down the small pores on the tray. At the same time, the low-pressure steam flows upward from the bottom of the stripper, the PVC slurry is subjected to heat transfer and mass transfer in the tray, and the VCM remaining outside the resin is precipitated. The low pressure steam and VCM gas are condensed from the top of the stripper into the condensation column and passed to the condensate tank to recover the VCM gas into the VCM gas cabinet.

The main parameters affecting the PVC stripping process or the stable operation of the stripper are temperature, the flow of steam and slurry, pressure, pressure difference and liquid level. Table 1 shows the values of the control parameters in a certain type of resin stripping. By analyzing the technique of the PVC stripping process, it has strong non-linearity and coupling characteristics. The main factors affecting the removal of vinyl chloride monomer in PVC are the top temperature of the stripping tower and the temperature at the bottom of the column. The factors affecting the temperature of the stripper are two main control quantities: the steam flow and the slurry flow, which are the main means of regulation in production process. However, due to the lack of effective mathematical model and strong coupling between variables, it is difficult to obtain satisfactory control effects. In this paper, an integrated modeling and hybrid intelligent control strategy based on neural network technology is proposed for the PVC stripping process.

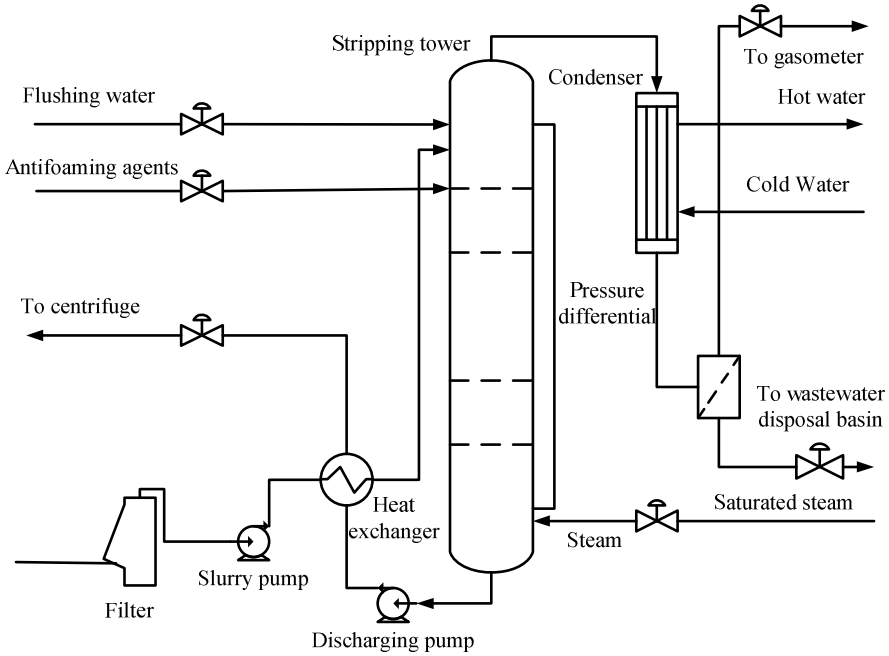

Fig. 1 Technique flowchart of PVC stripping process.

TABLE 1. CONTROL VALUES TO STRING TOWER PARAMETERS

Control points	Scope	Alarm range	Normal range	Real value
Temperature of tower top	0-150℃	Upper limit: 110℃ Lower limit: 70℃	80-105℃	85℃
Temperature of tower bottom	0-150℃	Upper limit: 130℃ Lower limit: 100℃	105-113℃	107℃
Pressure of tower top	0-0.1 MPa	Upper limit: 0.08 MPa Lower limit: 0.02 MPa	0.03-0.06 MPa	0.03 MPa
Pressure difference of Tower	0-60 MPa	Upper limit：30 MPa Lower limit：5 MPa	10-25 MPa	15 MPa
Intake steam flow	0-4000 kg/h	Upper limit: 3500 kg/h Lower limit: 1000 kg/h	1500-3000 kg/h	2200 kg/h
Inlet slurry flow	0-80 m^3/h	Upper limit：70 m^3/h Lower limit：15 m^3/h	35-50 m^3/h	40-45 m^3/h
Tower steam pressure	0-0.6 MPa	Upper limit：0.5 MPa Lower limit: 0.15 MPa	0.35-0.4 MPa	0.38 MPa

III. ADAPTIVE DECOUPLING CONTROL METHOD OF PVC STRIPPING PROCESS

A. Structure of Intelligent Decoupling Controller

The structure of the decoupling model proposed in this paper is shown in Fig. 2. The control system establishes two models for the slurry flow - stripping tower top temperature and the steam flow - striping bottom temperature. The entire control system consists of two open-loop decoupling controllers ENN1 and ENN2 established by two OSF-Elman neural networks and two PID controllers optimized by the Whale Optimization Algorithm (WOA).

In Fig. 2, $R_i(s)$ is the input quantity, $Y_i(s)$ is the output quantity and x_i represents the output of the PID controller, $U_i(s)$ represents the decouple output vector, and u_i' represents the control input vector ($i=1,2$). This method divides the establishment of the stripping decoupling model into two phases:

(1) Training stage. In the training stage, the controlled system is in an open loop state. Firstly, the OSF-Elman neural network (ENN1) is trained. At this time, ENN2 should be kept without input. The decoupling success flag is that the model corresponding to "slurry flow-striping top temperature" has no output, that is to say $Y_1(s)=0$. The parameters of ENN1 are adjusted when $Y_1(s)$ is a label for ENN1. The ENN2 is trained with the same method. Finally, the controlled object of the stripper is decoupled into two single-input single-output (SISO) systems, that is to say "slurry flow-stripper top temperature" and "steam flow-stripper bottom temperature".

(2) Control stage. Parameters of two PID controllers are online optimized by the identical WOA to achieve the closed-loop control of two single-input single-output systems. When the training process is completed, the trained weights and thresholds remain unchanged. The two systems are closed-loop controlled by using two PID controllers optimized by WOA. WOA is used to adjust the parameters K_p , K_i and K_d of the two PID controllers.

B. Elman Neural Network with Feedback of Output Layer Structure

1) Elman Neural Network

The Elman neural network is an important type of neural network. Because of the added feedback linkage among layers, it can represent the time delay between input and output, so the dynamic equations are adopted to carry out the description. The foreword network only implements the nonlinear mapping. On the other hand, it is precisely because of this feedback that the network has the ability of remember, so it has been widely used in many fields, such as sequence analysis, system identification, control, etc [11]. The structure model of the Elman neural network is shown in Fig. 3. In addition to the input layer, the output layer and the hidden layer, there is a special layer, the receiving layer (also known as the structural layer).

The structural unit is used to memorize the output of the units in the hidden layer at the previous moment, which can be considered as a delay operator. Therefore, the feed-forward connection part can perform the connection weight correction, but the recursive part is fixed so that it is not performed the learning correction.

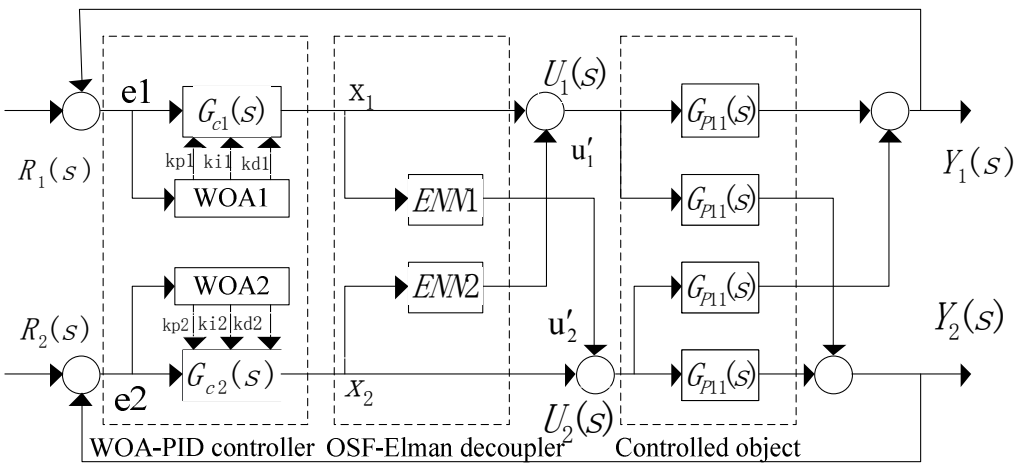

Fig. 2 Block diagram of PVC strippering process decoupling control system.

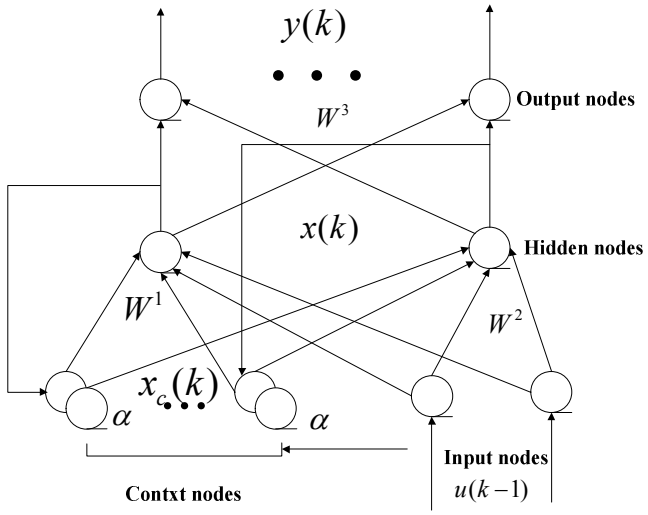

Fig. 3 Structure of Elman neural network .

2) Output-layer Structure Feedback Elman (OSF-Elman) Neural Network

In the standard Elman neural network, the function of the structure layer is too simple, because it just remembers the output value of the hidden layer at the last moment like a delay operator. Therefore, this paper introduces the feedback between the output layer and the receiving layer on the standard Elman neural network so as to make the entire network more rigorous without complex structure. The structure of the output-layer structure feedback Elman neural network (OSF-Elman) is shown in Fig. 4. It can be seen from Fig. 4 that the output of the receiving layer at time k is equal to the output of the hidden layer at time k -1 plus the output of the output layer.

$$x_{c,l}(k) = \alpha \bullet x_{c,l}(k-1) + x_l(k-1) \tag{1}$$

where, $l = 1, 2, \cdots, n$, $x_{c,l}$ is the output of the l th unit of the receiving layer, $x_l(k)$ is the output of the l th unit of the hidden layer, and α is the self-feedback factor.

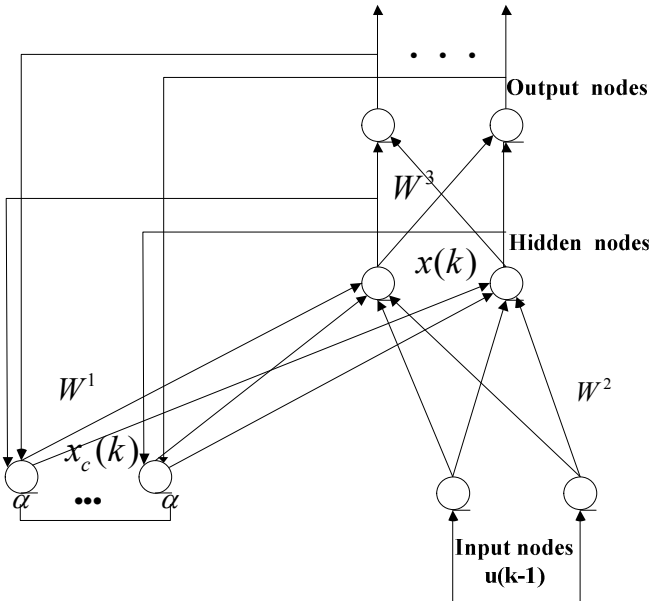

Fig. 4 Structure of OSF Elman neural network.

The mathematical model of the OSF-Elman neural network can be described as follows:

$$x(k) = f(W^1(x_c(k) + y(k)) + W^2 u(k-1)) \tag{2}$$

$$x_c(k) = \alpha \bullet (x_c(k-1) + y(k-1)) + x(k-1) \tag{3}$$

$$y_k = g(W^3 x(k)) \tag{4}$$

where, W^1 is the connection weight between the receiving layer and the hidden layer, W^2 is the connection weight between the input layer and the hidden layer, W^3 is the connection weight between the output layer and the hidden layer, $f(x)$ is a nonlinear activation function applied in hidden layer and $g(x)$ is a linear activation function generally used in the output layer. Their expressions are described as follows.

$$f(x) = \frac{1}{1+e^{-x}} \tag{5}$$

$$y_k = W^3 x(k) \tag{6}$$

where, y_k is the output of the OSF-Elman neural network.

3) Learning Algorithm of OSF-Elman Neural Network

Before defining the learning algorithm of the neural network, first give the error of the neural network:

$$E = \frac{1}{2}(y_d(k) - y(k))^T (y_d(k) - y(k)) \tag{7}$$

where $y_d(k)$ is the desired output and $y(k)$ is the actual output of the neural network. The partial derivative operation is carried out on W^3 in Eq. (7) to obtain:

$$\begin{aligned} \frac{\partial E}{\partial w_{ij}^3} &= -(y_{d,i}(k) - y(k)) \frac{\partial y_i(k)}{\partial w_{ij}^3} \\ &= -(y_{d,i}(k) - y(k)) g_i^{'}(\bullet) x_j(k) \end{aligned} \tag{8}$$

where w_{ij}^3 is the connection weight between the output layer unit and the hidden layer unit, $y_{d,i}$ is the expected output and y_i is the actual output of the neural network.

Assume $\delta_i^0 = (y_{d,i}(k) - y(k)) g_i^{'}(\bullet)$ and obtain:

$$\frac{\partial E}{\partial w_{i,j}^3} = -\delta_i^0 x_j(k) \tag{9}$$

where, $i = 1, 2, \cdots, m$, $j = 1, 2, \cdots, n$, $g_i^{'}(\bullet)$ is the activation function of the output layer unit, and the bias of the deviation E on W^2 can be expressed as:

$$\frac{\partial E}{\partial w_{ij}^2} = \frac{\partial E}{\partial x_j(k)} \frac{\partial y_i(k)}{\partial w_{ij}^2} = \sum_{i=1}^{m} (-\delta_i^0 w_{ij}^3) f_j^{'}(\bullet) u_q(k-1) \tag{10}$$

where, w_{ij}^2 represents the connection weight between the i th output of the input layer and the j th input of the hidden layer, $u_a(k-1)$ is the input of the input layer at the previous

moment and $f_i^{'}(\bullet)$ is the derivative of the activation function in the hidden layer.

Set $\delta_j^h = \sum(\delta_j^0 w_{ij}^3) f_j^{'}(\bullet)$ and obtain:

$$\frac{\partial E}{\partial w_{ij}^3} = -\delta_j^h u_q(k-1) \tag{11}$$

where, $j = 1,2,\cdots,n$, $q = 1,2,\cdots,r$.

Finally, the partial derivation of E on the connection weight W^1 among the hidden layer, the receiving layer and the output layer can be represented as:

$$\frac{\partial E}{\partial w_{jl}^1} = \sum_{i=1}^{m}(\delta_i^0 w_{ij}^3)\frac{\partial x_j(k)}{\partial w_{jl}^1} \tag{12}$$

where, $j = 1,2,\cdots,n$, $l = 1,2,\cdots,n$. w_{jl}^1 is the hybrid connection weight, that is to say it is the connection weight between the neurons of the output layer and the receiving layer, or between the neurons of the hidden layer and the receiving layer. The calculation expression of $\partial x_j(k)/\partial w_{jl}^1$ can be expressed as:

$$\begin{aligned}\frac{\partial x_j(k)}{\partial w_{jl}^1} &= \frac{\partial}{\partial w_{jl}^1}\left[f_j(\sum_{i=1}^{h} w_{jl}^1(x_{c,j}(k) + y_i(k-1)) + \sum_{i=1}^{r} w_{jl}^2 u_i(k-1))\right] \\ &= f_j^{'}(\bullet)\left[x_{c,j}(k) + y_i(k-1) + \sum w_{jl}^1 \frac{\partial x_{c,j}(k)}{\partial w_{jl}^1}\right]\end{aligned} \tag{13}$$

where, $x_{c,j}(k)$ is the output of the j th neuron in the receiving layer. It can be seen from the structural diagram of the OSF-Elman neural network that the relationship between $x_{c,j}(k)$ and w_{jl}^1 is negligible. Therefore, the above formula can be rewritten as:

$$\frac{\partial x_j(k)}{\partial w_{jl}^1} = f_j^{'}(\bullet)(x_{c,l}(k-1) + y_l(k-1)) \tag{14}$$

where, $x_j(k)$ is the output value of the j th neuron.

$$f_j^{'}(\bullet)x_{c,j}(k) = f_j^{'}(\bullet)(x_c(k-1) + y_l(k-1)) + \alpha f_j^{'}(\bullet)x_{c,j}(k) \tag{15}$$

Substitute Eq. (14) into Eq. (15) to obtain:

$$\frac{\partial x_j(k)}{\partial w_{jl}^1} = f_j^{'}(\bullet)(x_c(k-1) + y_l(k-1)) + \alpha\frac{\partial x_j(k-1)}{\partial w_{jl}^1} \tag{16}$$

By adopting $\Delta W = -\eta\dfrac{\partial E}{\partial w}$, the learning algorithm of Elman neural network can be described as:

$$\Delta w_{ij}^3 = \eta_1 \delta_i^0 x_j(k) \tag{17}$$

$$\Delta w_{jq}^2 = \eta_2 \delta_j^h u_g(k-1) \tag{18}$$

$$\Delta w_{ij}^1 = \eta_3 \sum_{i=1}^{m}(\delta_j^0 w_{ij}^3)\frac{\partial x_j(k)}{\partial w_{jl}^1} \tag{19}$$

where, $i = 1,2,\cdots,m$, $j = 1,2,\cdots,n$, $q = 1,2,\cdots,r$, $l = 1,2,\cdots,m$, η_1 , η_2 , and η_3 are the learning rates of W^1 , W^2 and W^3 .

$$\delta_i^0 = (y_{d,i}(k) - y(k))g_i^{'}(\bullet) \tag{20}$$

$$g_j^h = \sum(\delta_i^0 w_{ij}^3) f_i^{'}(\bullet) \tag{21}$$

4) Procedure of Establishing OSF-Elman Neural Network Decoupling Model

The steps of the OSF-Elman neural network decoupling algorithm are described as follows.

Step 1: Connect the neural decouple ENN1 and ENN2 with the controlled process.

Step 2: Initialize the all weights of the neural decouple, which is generally randomly initialized and requires the initial value to be small enough.

Step 3: Given input and ensure that the output data of the PID controller corresponds to the input data of the neural decouple.

Step 4: Calculate the output of the hidden layer, the output layer and the output layer by using Eq. (2)-(4) according to the number of samples and the given time interval.

Step 5: Calculate the weights increments of the output layer and the hidden layer by adopting Eq. (8), (10) and (12) to update W^3 , W^2 and W^1 .

Step 6: Repeat Step 4 and Step 5 until the specified number of iterations, and thereby determine W^3 , W^2 and W^1 .

The above updating strategy is used to train the weights of OSF-Elman neural network, which is equivalent that the dual input-dual output system is decoupled into two SISO nonlinear systems.

IV. Parameter Tuning of PID Controller Based on Whale Optimization Algorithm

The whale optimization algorithm (WOA) is a global optimization algorithm based on swarm intelligence technology inspired by the hunting behavior of humpback whales in 2016 [12]. This algorithm simulates three behaviors of the humpback whales (searching for prey, surrounding prey and preying with bubble nets). This paper uses the whale optimization algorithm to optimize the PID controller parameters.

A. Multivariable PID Decoupling Controller

The mathematical formula of the PID controller can be expressed as[13]:

$$u(t) = K_p\left[e(t) + \frac{1}{T_i}\int_0^t e(t)dt + \frac{T_d de(t)}{dt}\right] \tag{22}$$

where, $K_i = K_P/T_i$, $K_d = K_p T_d$, and $e(t)$ is the feedback deviation.

The OSF-Elman neural network is used to eliminate the coupling between the channels of the original coupling system. WOA is adopted to optimize the control parameters of the PID controller. The structure is shown in Fig. 2.

B. Coding and Fitness Function

The parameters of the PID controller are optimized by using WOA for obtaining better control effects. In view of the fact that the PID controller design is actually a multidimensional function optimization problem, WOA adopts the real number coding method. For the PVC stripping process, the parameters of the muti-variable PID controllers can be directly coded as:

$$\text{PID1:}\ X_1 = \{k_{p1}, k_{i1}, k_{d1}\},\ \text{PID2:}\ X_2 = \{k_{p2}, k_{i2}, k_{d2}\} \quad (23)$$

The optimization of the controller parameters is designed to make the overall control deviation of the system tend to zero, have a faster response speed and a smaller overshoot. In this paper, the integrated time absolute error (ITAE) is used in the simulation experiments.

$$ITAE = \int_0^\infty t|e(t)|dt \quad (24)$$

C. Parameter Searching Space

The searching space of WOA is centered on the parameters obtained by the Ziegler-Nichols (Z-N) method, and is extended to the left and right sides so that the reasonable kernel of the Z-N method can be fully utilized and the searching space of the actual parameters is reduced. If the optimal solution of the parameters is very close to the boundary of the searching space, it should be further expanded based on the solution and a new round of searching is conducted.

$$(1-\alpha) * K_P' \le K_P \le (1+\alpha) * K_P' \quad (25)$$

$$(1-\alpha) * K_i' \le K_i \le (1+\alpha) * K_i' \quad (26)$$

$$(1-\alpha) * K_d' \le K_d \le (1+\alpha) * K_d' \quad (27)$$

where, (K_P, K_i, K_d) are the PID controller parameters, (K_P', K_i', K_d') are the tuned parameters based on the Z-N method, and α is a predetermined value in [0, 1].

V. Simulation Experiments and Results Analysis

A. OSF-Elman NN Modeling on PVC Stripping Process

In order to verify the effectiveness of the proposed algorithm, 280 sets of data in the PVC stripping process were collected to train the OSF-Elman neural network model, and 80 sets of data from another batch were selected as test samples to verify the validity of the trained model. In this paper, the OSF-Elman neural network model is established to model the relationship between the tower top temperature of the stripper and the slurry flow. The simulation results of the tower top temperature Y1 using an unmodified Elman neural network are shown in Fig. 5 and Fig. 6. Fig. 5 is a comparison of the predicted output of the training data with the actual output, and Fig. 6 is the predicted output and actual data for the testing data. The simulation results of the tower top temperature Y1 using an OSF-Elman neural network are shown in Fig. 7 and Fig. 8. Fig. 7 is a comparison of the predicted output of the raining data with the actual output, and Fig. 8 is the predicted output and actual data for the testing data. It can be seen from Fig. 5 that the model established by the original Elman neural network clearly inherits the shortcomings of the BP network, and a partial over-fitting phenomenon occurs. It can be seen from Fig. 6 that the prediction effect of the test data is obviously not as good as that of Fig. 8. It can be seen from Fig. 6 that the model established by the OSF-Elman neural network effectively jumps over-fitting, and the established model has certain generalization ability. Therefore, seen from Fig. 8, the prediction effect is better than that of Fig. 5 when the test data is simulated. The simulation results of the tower bottom temperature Y2 using an unmodified Elman neural network are shown in Fig. 9 and Fig. 10.

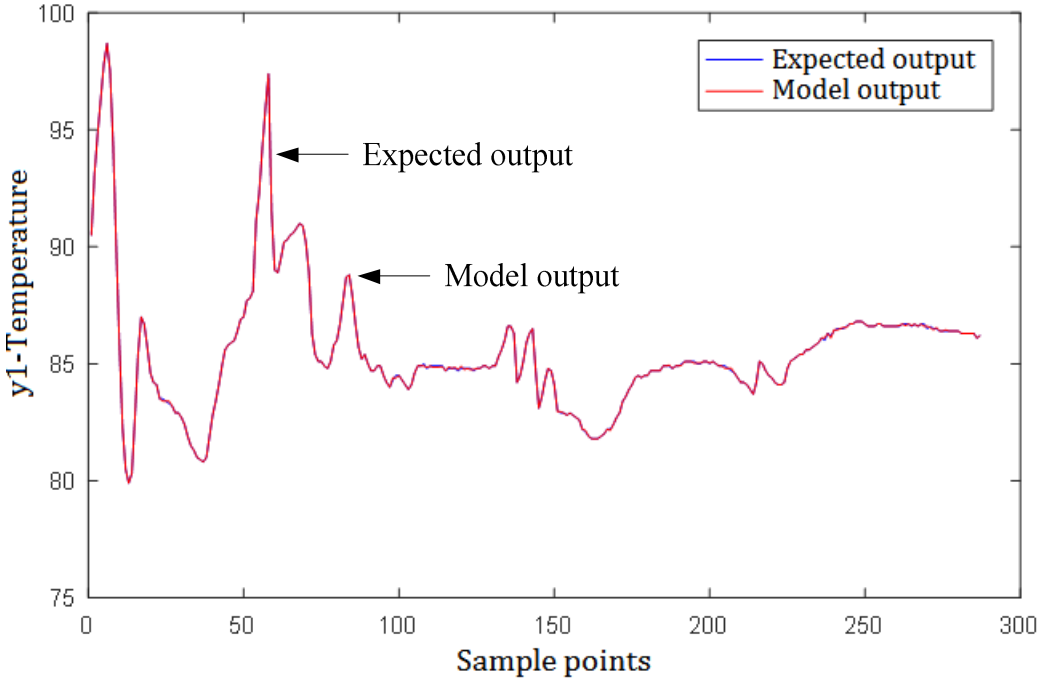

Fig. 5 Simulation results of Elman NN model on tower top temperature (Training data).

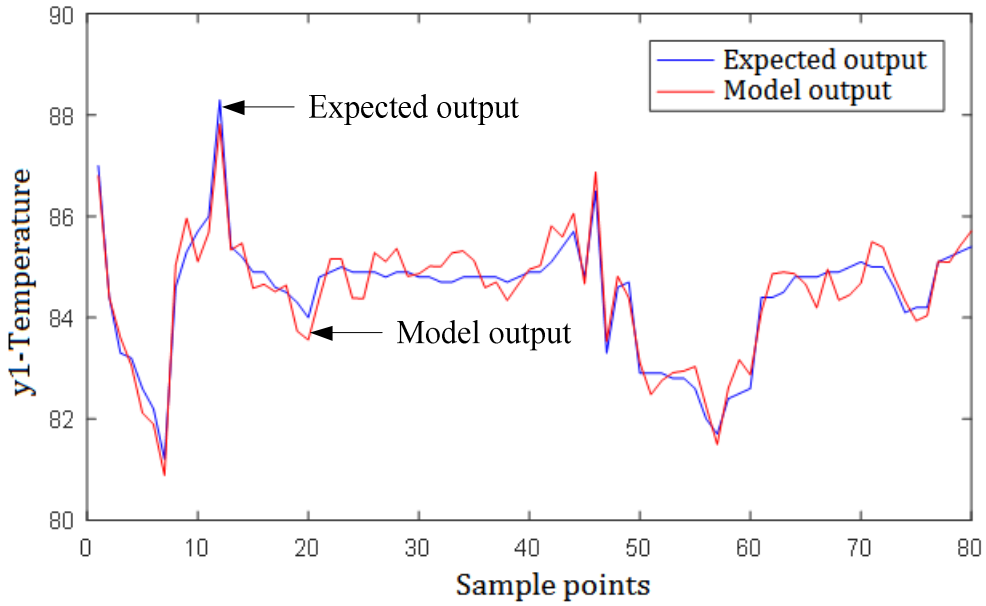

Fig. 6 Simulation results of Elman NN model on tower top temperature (Testing data).

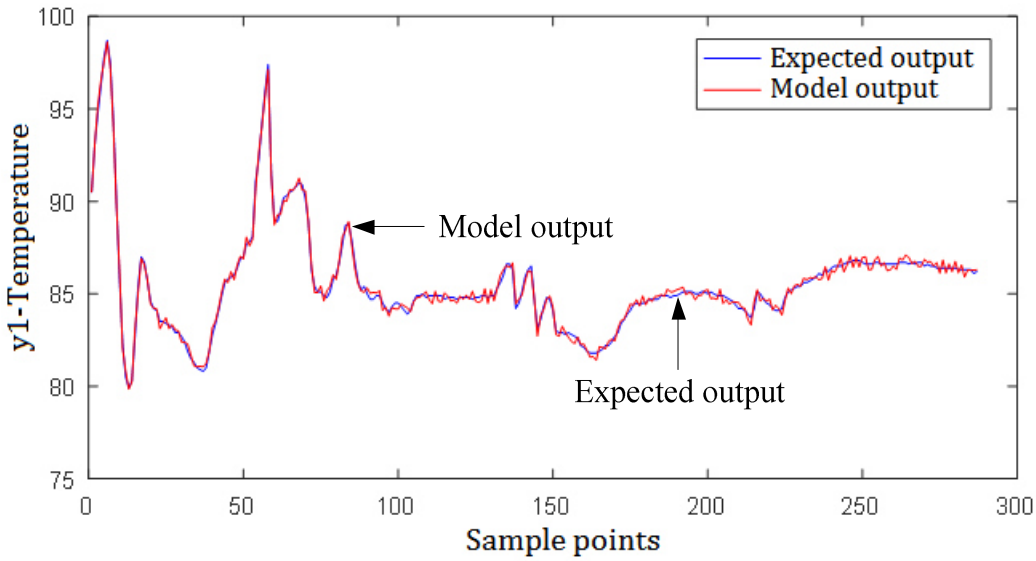

Fig. 7 Simulation results of OSF-Elman NN model on tower top temperature (Training data).

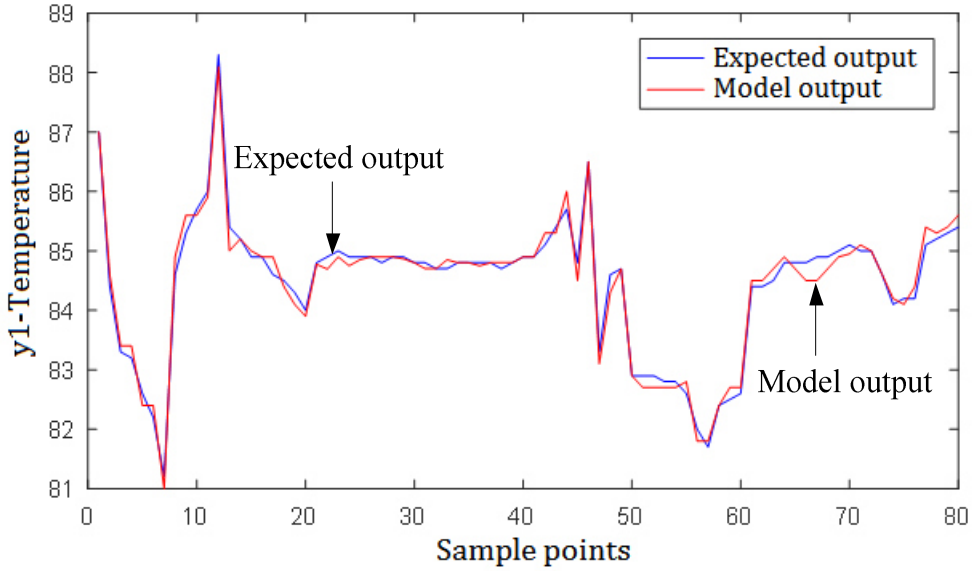

Fig. 8 Simulation results of OSF-Elman NN model on tower top temperature (Testing data).

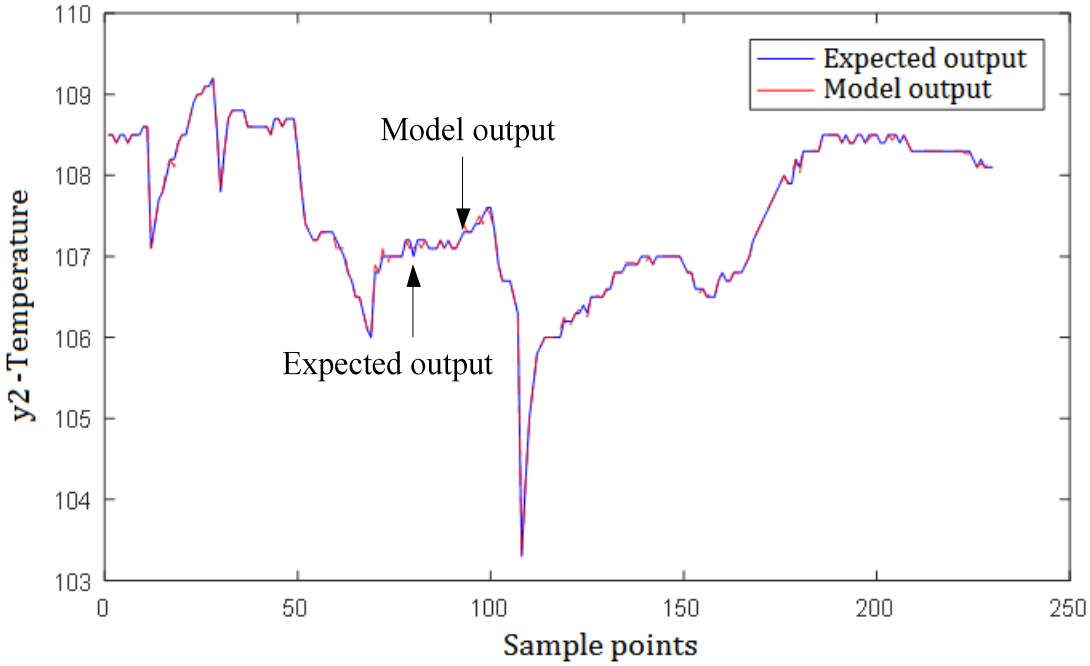

Fig. 9 Simulation results of Elman NN model on tower bottom temperature (Training data).

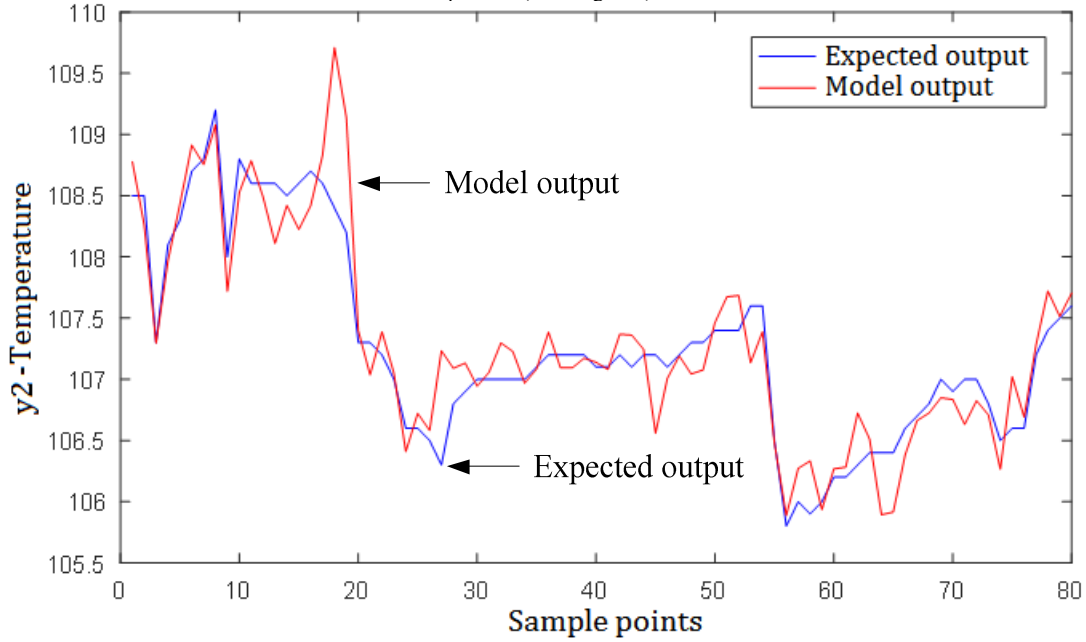

Fig. 10 Simulation results of Elman NN model on tower bottom temperature (Testing data).

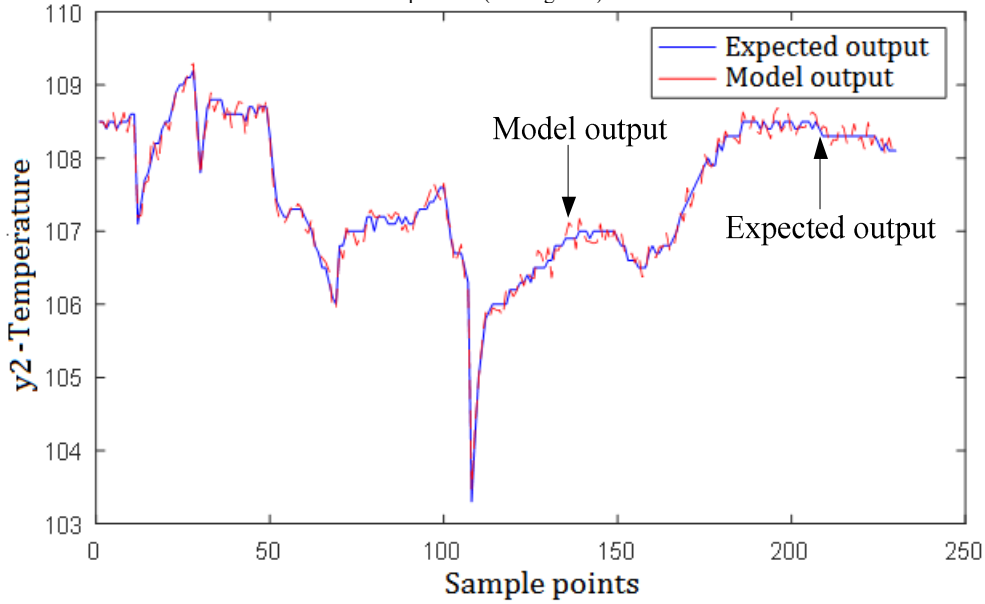

Fig. 11 Simulation results of OSF-Elman NN model on tower bottom temperature (Training data).

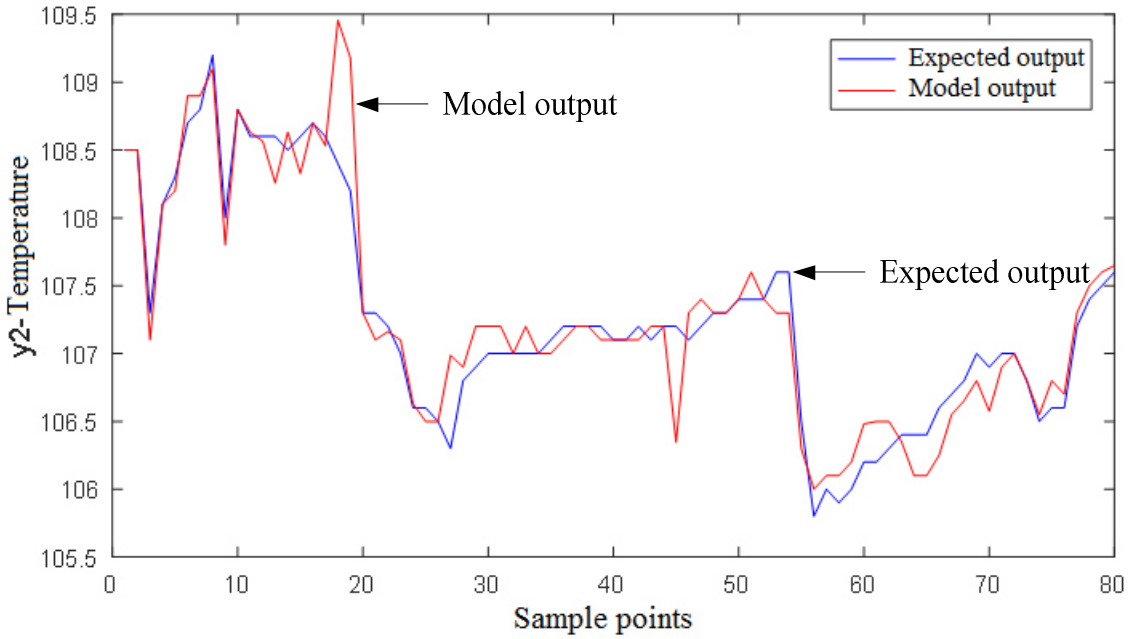

Fig. 12 Simulation results of OSF-Elman NN model on tower bottom temperature (Testing data).

Fig. 9 is a comparison of the predicted output of the training data with the actual output, and Fig. 10 is the predicted output and actual data for the testing data. The simulation results of the tower bottom temperature Y2 using an OSF-Elman neural network are shown in Fig. 11 and Fig. 12. Fig. 11 is a comparison of the predicted output of the training data with the actual output, and Fig. 12 is the predicted output and actual data for the testing data. It can be seen from Fig. 9 and Fig.10 that when the Elman neural network is adopted to model the tower bottom temperature, the phenomenon of over-fitting also appears, which thus seriously affects the decoupling effect of the decouples. Seen from Fig. 11 and Fig. 12, the adoption of the OSF-Elman neural network can effectively weakens the over-fitting phenomenon of the original Elman neural network and effectively improves the generalization ability of the model.

B. Stability Analysis of Decoupling Controller

In order to verify the effectiveness of the decoupling model established by the OSF-Elman neural network, the control performance was verified by the simulation experiments. The parameters setting of the model are described as follows. The OSF-Elman neural network has five units in the input layer, six units in the hidden layer and one unit in the output layer. The learning rate of the OSF-Elman neural network is 0.8. For the adopted WOA to optimize the parameters of the PID controller, the number of search agents is 30, the number of iterations is 1000, the search path selects the logarithmic spiral curve, and other parameters are randomly set at the initialization stage. It is known from the actual engineering experience that the temperature at the tower top is generally 85 °C, but it must not be higher than 110 °C. Otherwise, the PVC will be decomposed. Therefore, the standard signal of the temperature at the tower top is set to 85 °C. The optimum temperature at the tower bottom is 107 ° C, and generally cannot be higher than 113 ° C. In order to take into account the situation that occurred in the actual PVC stripping process as much as possible, this paper simulates the situation of external disturbance. The simulation results are shown in Fig. 13 and Fig. 14.

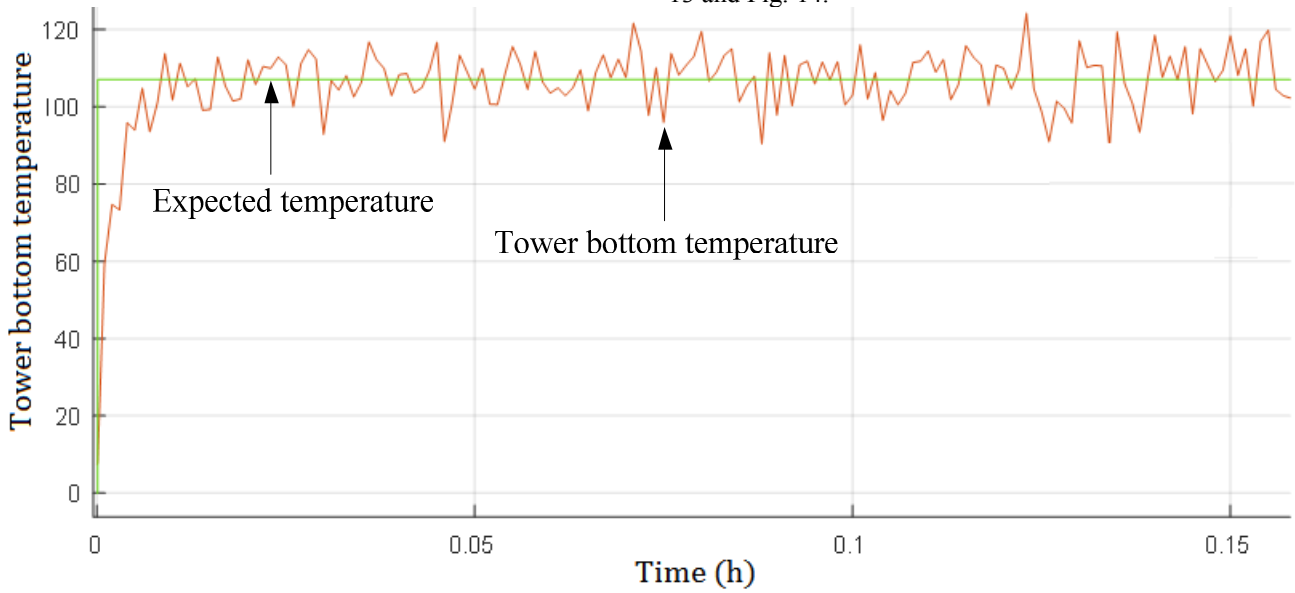

(a) Tower bottom temperature curves under disturbance

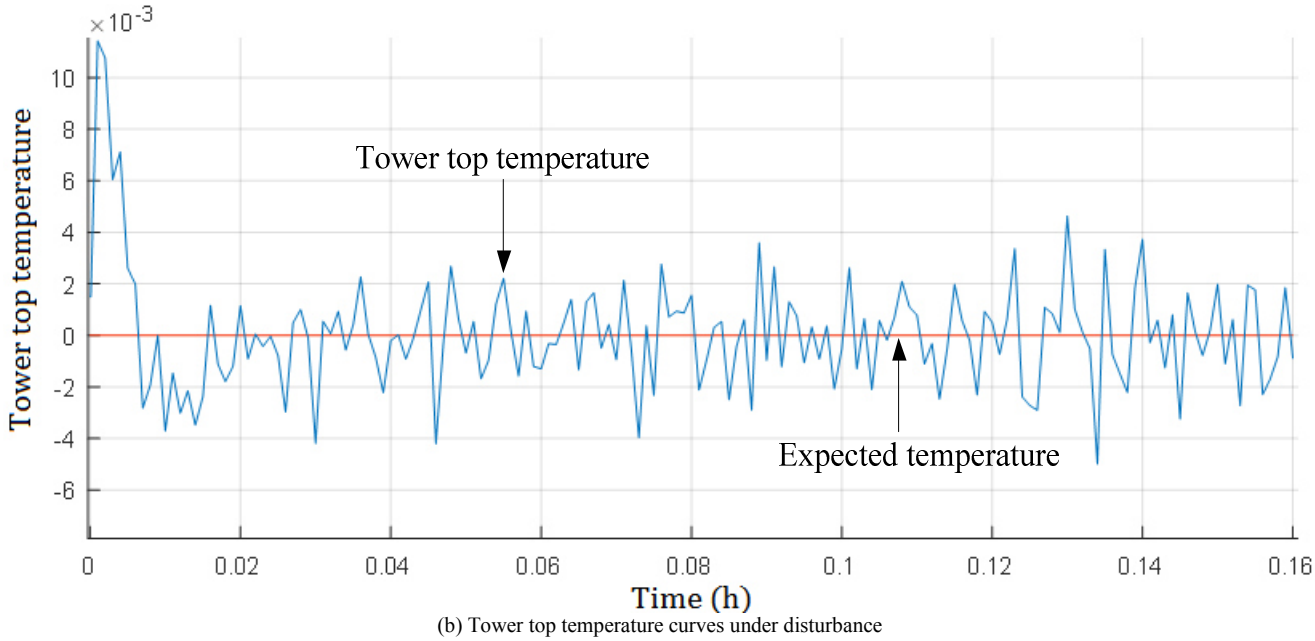

(b) Tower top temperature curves under disturbance

Fig. 13 Tower bottom temperature under disturbance.

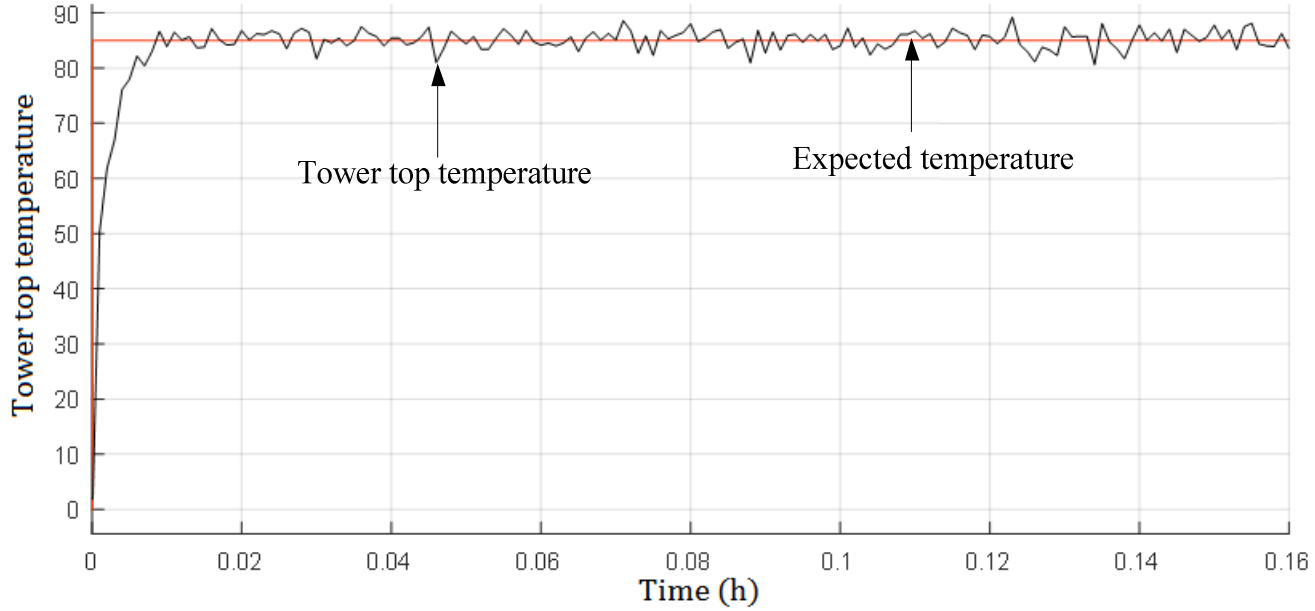

(a) Tower top temperature curves under disturbance

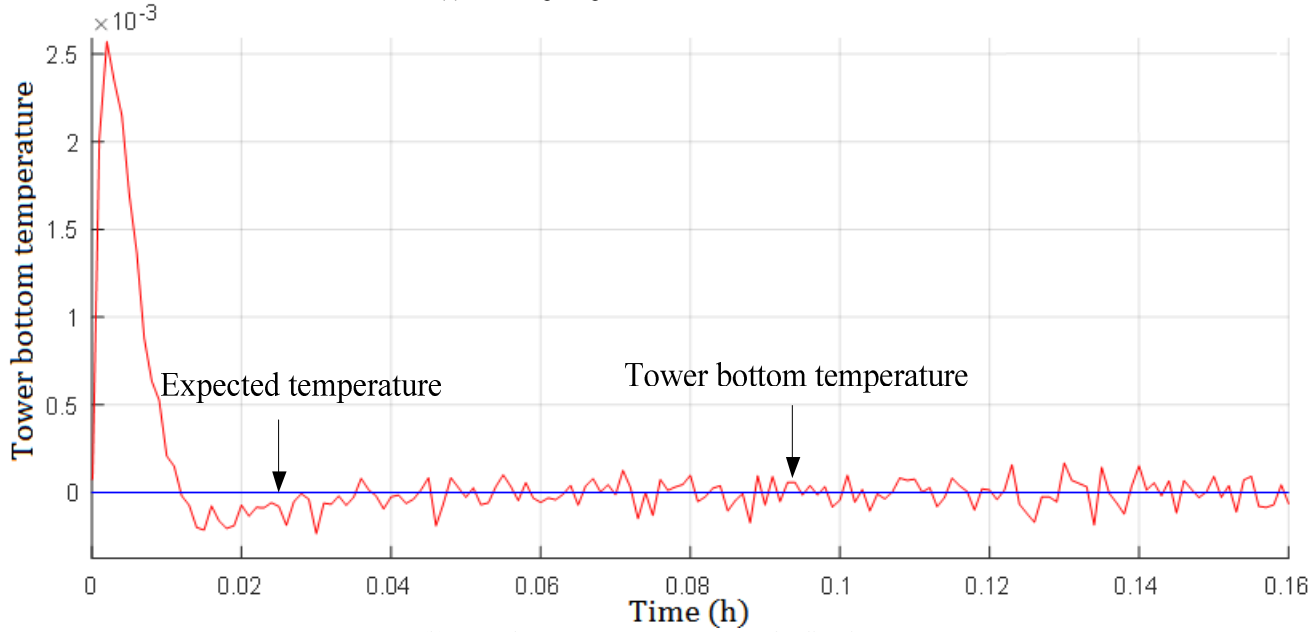

(b) Tower bottom temperature curves under disturbance

Fig. 14 Tower top temperature under disturbance.

It can be seen from the above simulation results that it has been basically achieved to decouple the temperature at the tower bottom and the tower top. At this time, the temperature at the top of the tower fluctuates around zero degree. Then the simulation experiments are carried out on the temperature at the top of the tower. It can be seen from Fig. 14 that the temperature at the top of the tower begins to change after the introduction of the disturbance, but it still floats around 85 degree. At the same time, the temperature at the bottom of the tower floats at zero degree. That is to say that the system has a certain anti-interference ability and achieves the satisfied decoupling result at the same time.

VI. Conclusion

The PVC stripping process is highly nonlinear and time varying, and is a complex nonlinear industrial process. In this paper, the improved Elman neural network (OSF-Elman NN) is adopted to model the PVC stripping process with the actual operational data. The parameters of the PID controller are optimized by using whale optimization algorithm (WOA). Simulation results verify the effectiveness of the proposed integrated control strategy.

References

[1] J. S. Wang, S. Hanm, and Q. P. Guo, "Echo State Networks Based Predictive Model of Vinyl Chloride Monomer Convention Velocity Optimized by Artificial Fish Swarm Algorithm," *Soft Computing*, vol. 18, no. 3, pp. 457-468, 2014.

[2] Z. G. Hui, "The Application of Stripping Technology in the Production of PVC," *Polyvinyl Chloride*, vol. 7, no. 2, pp. 8-12, 2007.

[3] H. Li, "Design of Multivariable Fuzzy-neural Network Decoupling Controller," *Control and Decision*, vol. 21, no. 5, pp. 593-596, 2006.

[4] W. G. Xiao, Z. M. Wang, Y. F. Guo, and S. Q. Chen, "PVC Boiling Bed Drying Process Optimization Control System," *Automation and Instruments in Chemical Industry*, vol. 21, no. 5, pp. 12-15, 1994.

[5] K. S. Lee, and J. H. Lee, "Model Predictive Control for Nonlinear Batch Processes with Asymptotically Perfect Tracking," *Computers & Chemical Engineering*, vol. 21, no. 10, pp. 873-879, 1997.

[6] Whei-Min Lin, and Chih-Ming Hong, "A New Elman Neural Network-based Control Algorithm for Adjustable-pitch Variable-speed Wind-energy Conversion Systems," *IEEE Transactions on Power Electronics*, vol. 26, no. 2, pp. 473-481, 2011.

[7] X. Z. Gao, S. J. Ovaska, "Genetic Algorithm Training of Elman Neural Network in Motor Fault Detection," *Neural Computing & Applications*, vol. 11, no. 11, pp. 37-44, 2002.

[8] C. Tan, N. Qi, X. Zhou, X. H. Liu, X. G. Liu, Z. B. Wang, and L. Si, "A Pressure Control Method for Emulsion Pump Station Based on Elman Neural Network," *Computational Intelligence & Neuroscience*, vol. 2015, pp. 1-8, 2015.

[9] D. S. Li, Q. He, and Y. Chen, "Velocity Control of Longitudinal Vibration Ultrasonic Motor Using Improved Elman Neural Network Trained by CQPSO with Lévy Flights," *Journal of Vibroengineering*, vol. 16, no. 2, pp. 735-747, 2014.

[10] J. F. Qiao, X. C. Yuan, and H. G. Han, "Self-organising T-S Fuzzy Elman Network Based on EKF," *Control & Decision*, vol. 29, no. 5, pp. 853-859, 2014.

[11] X. H. Shi, Y. C. Liang, H. P. Lee, W. Z. Lin, and S. P. Lim, "Improved Elman Networks and Applications for Controlling Ultrasonic Motors," *Applied Artificial Intelligence*, vol. 18, no. 7, pp. 603-629, 2004.

[12] S. Mirjalili, and A. Lewis, "The Whale Optimization Algorithm," *Advances in Engineering Software*, vol. 95, pp. 51-67, 2016.

[13] J. S. Wang, and S. X. Li, "PID Decoupling Controller Design for Electroslag Remelting Process Using Cuckoo Search Algorithm with Self-tuning Dynamic Searching Mechanism," *Engineering Letters*, vol. 25, no. 2, pp. 125-133, 2017.

Hong-Yu Wang is a postgraduate student in the School of Electronic and Information Engineering, University of Science and Technology Liaoning, Anshan, 114051, PR China. His main research interest is modeling and control methods of industrial process.

Dong Wei is with the School of Electronic and Information Engineering, University of Science and Technology Liaoning, Anshan, 114051, PR China. His main research interest is modeling and intelligent control of complex industry process.

Jie-Sheng Wang received his B. Sc. And M. Sc. degrees in control science from University of Science and Technology Liaoning, China in 1999 and 2002, respectively, and his Ph. D. degree in control science from Dalian University of Technology, China in 2006. He is currently a professor and Doctor's Supervisor in School of Electronic and Information Engineering, University of Science and Technology Liaoning. His main research interest is modeling of complex industry process, intelligent control and Computer integrated manufacturing.

Wei-Zhen Sun is a postgraduate student in the School of Electronic and Information Engineering, University of Science and Technology Liaoning, Anshan, 114051, PR China. His main research interest is modeling and control methods.